CMS Physics Analysis Summary

Contact: cms-phys-conveners-ftr@cern.ch 2018/11/19

Constraints on the Higgs boson self-coupling from ttH+tH, $H \to \gamma\gamma$ differential measurements at the HL-LHC

The CMS Collaboration

Abstract

This note details a study of prospects for ttH+tH, $H \to \gamma\gamma$ differential cross section measurements at the HL-LHC with the CMS Phase-2 detector. The study is performed using simulated proton-proton collisions at a centre-of-mass energy of $\sqrt{s} = 14$ TeV, corresponding to 3 ab^{-1} of data. The expected performance of the upgraded CMS detector is used to model the object reconstruction efficiencies under HL-LHC conditions. The results are interpreted in terms of the expected sensitivity to deviations of the Higgs boson self-coupling, κ_λ, from beyond standard model effects. Using the HL-LHC data, the precision expected in ttH+tH, $H \to \gamma\gamma$ differential cross section measurements will constrain κ_λ within the range $-4.1 < \kappa_\lambda < 14.1$, at the 95% confidence level, assuming all other Higgs boson couplings are fixed to standard model predictions. Moreover, it is possible to disentangle the effects of a modified Higgs boson self coupling from the presence of other anomalous couplings by using the differences in the shape of the measured spectrum. This separation is unique to differential cross section measurements. The ultimate sensitivity to the Higgs boson self coupling, achievable using differential cross section measurements, will result from a combination across Higgs boson production modes and decay channels.

1 Introduction

In the standard model (SM) of particle physics [1–6], electroweak symmetry breaking (EWSB) is realised through the addition of a complex scalar doublet field, which, after EWSB, yields a physical, neutral, scalar particle, a Higgs boson (H). Since the discovery of the Higgs boson by the ATLAS and CMS Collaborations [7–9], several experimental measurements have been designed to test its compatibility with SM predictions. Despite the precision already achieved in measurements of the Higgs boson couplings to SM particles in the first two runs of the LHC [10–12], constraints on the Higgs boson self-coupling obtained from searches for double Higgs boson production [13, 14], remain limited.

An alternative approach to probing the Higgs boson self-coupling, exploiting radiative corrections to inclusive and differential Higgs boson production rates has been suggested in references [15–20]. At next-to-leading order (NLO), single-Higgs boson production includes processes with access to the Higgs boson trilinear coupling, λ_3, such as that shown in Fig. 1. The contributions from the Higgs boson self-coupling are sizeable for Higgs boson production in association with a pair of top quarks (ttH), a single top-quark (tH) or a massive vector boson (VH, V=W or Z). The effect is larger in these production modes due to the large mass of the V boson or top quark, providing a larger coupling to the virtual Higgs boson. Conversely, corrections to the dominant gluon-fusion (ggH) and vector-boson fusion (qqH) production modes are much smaller. Differential cross section measurements, in particular as a function of the Higgs boson transverse momentum $p_{\mathrm{T}}^{\mathrm{H}}$, allow one to disentangle the effects of modified Higgs boson self-coupling values from other effects such as the presence of anomalous top–Higgs couplings.

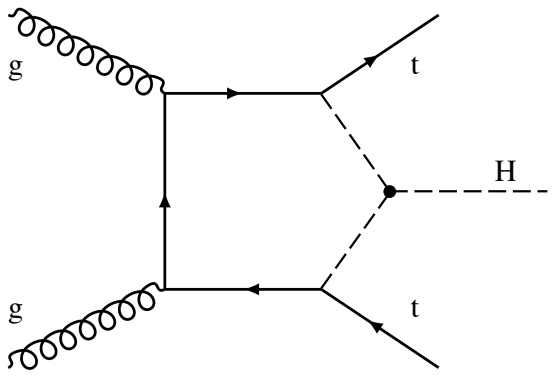

Figure 1: Example of a NLO Feynman diagram for ttH production which includes the Higgs boson self-coupling.

The dependence of the single-Higgs boson differential cross section is parameterised as a function of $\kappa_\lambda = \lambda_3/\lambda_3^{\mathrm{SM}}$, by considering NLO terms arising from the Higgs boson self-coupling such as the one in Fig. 1. This dependance is sensitive to both the production mode and kinematics of the Higgs boson. Scaling functions, $\mu_{ij}(\kappa_\lambda)$, are calculated using an electroweak reweighting tool [21] which determines the cross section, relative to the SM prediction, in a specific bin, i, of $p_{\mathrm{T}}^{\mathrm{H}}$, for each production mode, j. The κ_λ-dependent modifications are largest for ttH production, at threshold (low $p_{\mathrm{T}}^{\mathrm{H}}$). A 20% enhancement to the ttH production rate for $p_{\mathrm{T}}^{\mathrm{H}} \in [0,45]$ GeV, is predicted for $\kappa_\lambda \sim 10$. Further details on extracting $\mu_{ij}(\kappa_\lambda)$ relevant for this analysis, and the electroweak reweighting tool is provided in Section 3.

This note describes a strategy for measuring the $p_{\mathrm{T}}^{\mathrm{H}}$ differential cross section of a Higgs boson produced in association with at least one top quark and decaying to photons (ttH + tH, $\mathrm{H} \to \gamma\gamma$), at the High-Luminosity LHC (HL-LHC) with the CMS Phase-2 detector, for a centre-

of-mass energy of $\sqrt{s} = 14\,\text{TeV}$. The $\text{H} \to \gamma\gamma$ decay mode provides a clean final state in which the transverse momentum of the Higgs boson can be well reconstructed, owing to the excellent energy resolution of the CMS electromagnetic calorimeter for photons. Moreover, measurements of ttH production [22, 23] from a combination of decay channels obtain a significant contribution in sensitivity from the $\text{H} \to \gamma\gamma$ decay. The expected precision is determined based on simulated proton-proton (pp) events at the HL-LHC in which the conditions of the HL-LHC runs are accounted for in the object reconstruction performance of the upgraded CMS detector. The measurements are used to extract a constraint on the Higgs boson self-coupling which will be obtainable in this channel with the full HL-LHC dataset of $3\,\text{ab}^{-1}$.

This note is organised as follows: a summary of the upgraded CMS detector is provided in Section 2. Section 3 describes the simulated event samples and the parameterisation of the expected performance of the CMS Phase-2 detector. Section 4 describes the event selection optimised for the $\text{ttH} + \text{tH}$, $\text{H} \to \gamma\gamma$ differential cross section measurement. Section 5 describes the event categorisation and strategy for the signal and background modelling. Finally, the results are presented in Section 6.

2 The CMS Phase-2 detector

The CMS detector [24] will be substantially upgraded in order to fully exploit the physics potential offered by the increase in luminosity at the HL-LHC [25], and to cope with the demanding operational conditions at the HL-LHC [26–31].

The upgrade of the first level hardware trigger (L1) will allow for an increase of L1 rate and latency to about 750 kHz and 12.5 μs, respectively, and the high-level software trigger (HLT) is expected to reduce the rate by about a factor of 100 to 7.5 kHz.

The entire pixel and strip tracker detectors will be replaced to increase the granularity, reduce the material budget in the tracking volume, improve the radiation hardness, and extend the geometrical coverage and provide efficient tracking up to pseudorapidities of about $|\eta| = 4$. The muon system will be enhanced by upgrading the electronics of the existing cathode strip chambers (CSC), resistive plate chambers (RPC) and drift tubes (DT). New muon detectors based on improved RPC and gas electron multiplier (GEM) technologies will be installed to add redundancy, increase the geometrical coverage up to about $|\eta| = 2.8$, and improve the trigger and reconstruction performance in the forward region.

The barrel electromagnetic calorimeter (ECAL) will feature the upgraded front-end electronics that will be able to exploit the information from single crystals at the L1 trigger level, to accommodate trigger latency and bandwidth requirements, and to provide 160 MHz sampling allowing high precision timing capability for photons. The hadronic calorimeter (HCAL), consisting in the barrel region of brass absorber plates and plastic scintillator layers, will be read out by silicon photomultipliers (SiPMs). The endcap electromagnetic and hadron calorimeters will be replaced with a new combined sampling calorimeter (HGCal) that will provide highly-segmented spatial information in both transverse and longitudinal directions, as well as high-precision timing information.

Finally, the addition of a new timing detector for minimum ionizing particles (MTD) in both barrel and endocap region is envisaged to provide capability for 4-dimensional reconstruction of interaction vertices that will allow to significantly offset the CMS performance degradation due to high PU rates.

A detailed overview of the CMS detector upgrade program is presented in Ref. [26–31], while

the expected performance of the reconstruction algorithms is summarised in Ref. [32].

3 Event generation and detector simulation

Simulated ttH events are produced using POWHEG v2.0 [33, 34] at NLO. Additional contributions from Higgs boson production via gluon-fusion (ggH), in association with a vector boson (VH), and in association with a single top (tH) and a quark jet (tHq) or a W boson (tHW) are generated using MADGRAPH5_aMC@NLO v2.2.2 [35], interfaced with PYTHIA v8.205 [36], at NLO. The inclusive cross sections of ttH, tH, and VH production are calculated to NLO precision in quantum chromodymanics (QCD) and electroweak (EW) theory [37], while the ggH cross section is calculated to next-to-next-to-next-to-leading order (N^3LO) precision in QCD and NLO precision in EW theory [38].

The irreducible background arises from top pair production in which two photons are radiated ($tt + \gamma\gamma$). Reducible backgrounds from top pair production in which one photon is radiated ($tt + \gamma$) and inclusive top pair production ($t\bar{t}$), where additional jets in the events are misidentified as isolated photons, contribute due to their larger cross sections. Simulated $tt + \gamma\gamma$ and $tt + \gamma$ events are generated using MADGRAPH5_aMC@NLO v2.2.2, while the inclusive $t\bar{t}$ sample is produced using POWHEG v2.0. In both cases, the events are interfaced with PYTHIA v8.205 for hadronisation and showering. Further backgrounds arise from events in which two isolated photons are produced ($\gamma - \gamma$) or in which one photon is reconstructed from a hadronic shower which has been misidentified as a photon ($\gamma - j$). The $\gamma - \gamma$ sample is generated using SHERPA v2.2.5 [39] while the $\gamma - j$ sample is generated with PYTHIA v8.205.

The signal and background events are processed with DELPHES [40] to simulate the response of the CMS Phase-2 detector to showered particles. The object reconstruction and identification efficiencies, and the detector response and resolution are parameterised using events simulated with GEANT4 [41]. The mean number of simulated interactions per bunch crossing (pile-up) is set to 200 to model the expected conditions for pp collisions at the HL-LHC.

In DELPHES, photons are reconstructed as clusters of energy in the electromagnetic calorimeter, with no matching hits in the tracker. The photon reconstruction efficiency and fake rate are parametrised in accordance with a tight working point requirement on the photon identification score [42], available in the GEANT4 simulation. Generator-level muons and electrons from the interaction are reconstructed with some p_T and η dependent probability. These probabilities vanish outside of the tracker acceptance and below some energy threshold.

Hadronic jets are reconstructed using the CMS particle-flow (PF) algorithm [43], which uses information from the calorimeters and tracker in DELPHES. The output jet is a result of clustering the smeared particle-flow tracks and the particle-flow towers, using the common anti-k_T algorithm [44], with a distance parameter of 0.4. For clustering, the FastJet package [45] is used and the PUPPI algorithm is employed to partially clean the effects of pile-up [46]. To identify jets originating from the hadronization of b quarks, a variable is constructed to match the performance of the DeepCSV algorithm [47], at different working points. This variable uses a parametric formula for the b tagging probability, which depends on the p_T, η and truth-level parton flavour of the jet. A medium working point is used in this analysis, which corresponds to a 79% efficiency for true b jets with p_T = 100 GeV, in the central region of the detector, and a misidentification probability of around 1.5% for jets originating from light quarks and gluons. The discriminant incorporates the expected improvements with the planned Phase-2 MTD [31].

The missing transverse momentum, p_T^{miss}, is taken as the negative vector p_T sum of all recon-

structed objects in DELPHES after employing the PUPPI algorithm to mitigate the effects of pile-up. The scalar p_{T} sum of all reconstructed objects, after the PUPPI algorithm corrections, is labelled as S_T.

To extract the signal scaling functions, $\mu_{ij}(\kappa_\lambda)$, leading order (LO) parton-level ttH, tH and VH events are generated using MADGRAPH5_aMC@NLO v2.5.5. These events are used as input to the electroweak reweighting tool, described in Ref. [21], which calculates λ_3-dependent corrections at NLO, $\mathcal{O}(\lambda_3)$, by reweighting events on an event-by-event basis. A diagram filter is applied to select only the relevant one-loop matrix elements which feature the trilinear coupling. The κ_λ dependence is determined by taking the ratio of the $\mathcal{O}(\lambda_3)$ to LO contributions in bins of the generator-level $p_{\mathrm{T}}^{\mathrm{H}}$ spectrum, and feeding into the scaling equations provided in Ref. [16].

4 Event selection

To identify the $\mathrm{H} \to \gamma\gamma$ final state, events are required to have two photons in the invariant mass range: $100 < m_{\gamma\gamma} < 180$ GeV, such that the leading (sub-leading) photon satisfies $p_{\mathrm{T}}^{\gamma}/m_{\gamma\gamma} > 1/3$ (1/4). The photons must lie within pseudorapidity, $|\eta^{\gamma}| < 2.4$, excluding the barrel-endcap transition region: $1.44 < |\eta^{\gamma}| < 1.57$. The two candidate photons are also required to be separated by $\Delta R_{\gamma\gamma} > 0.4$. Additionally, the photons must satisfy an isolation requirement such that the sum of charged transverse momentum in a cone of radius $\Delta R_{\gamma} = 0.4$, centred on the photon candidate, is less than $0.3\, p_{\mathrm{T}}^{\gamma}$. If more than two photons pass the above criteria, then the pair with $m_{\gamma\gamma}$ closest to 125 GeV is chosen.

Top quark decay products in the final state are used to select events consistent with originating from ttH or tH production. The top quark decays almost exclusively to a bottom quark and a W boson, hence, the selection requires all events to have at least one b tagged jet. Two orthogonal selection criteria are then imposed to distinguish between the possible final states of the W boson decay. The hadronic channel describes the situation in which all W bosons decay to a quark-antiquark pair, and the leptonic channel is designed to be enriched in events where at least one W boson decays leptonically, to the electron + neutrino ($\mathrm{e}\nu$) or muon + neutrino ($\mu\nu$) final states.

In the hadronic channel, events must contain at least 3 jets, separated by $\Delta R > 0.4$ with respect to both photon candidates. The jets are required to have $p_{\mathrm{T}} > 25$ GeV, and to lie inside the region $|\eta| < 4$. Note, this pseudorapidity requirement incorporates the improved tracker coverage of the CMS Phase-2 detector. Additionally, a leptonic veto is applied to discard any events with at least one isolated electron or muon. Here, isolated leptons are required to have $p_{\mathrm{T}} > 20$ GeV and $|\eta| < 2.4$, excluding the barrel-endcap transition region for electrons. Muons must satisfy a similar isolation requirement to photons, such that the sum of all reconstructed particles p_{T}, inside a cone of radius $\Delta R = 0.4$, excluding the muon itself, is less than 0.25 times the transverse momentum of the muon. In addition, for electrons, the invariant mass of the electron-photon pairs, $m_{\mathrm{e}\gamma}$, is required to be greater than 5 GeV from the Z boson mass.

The selection criteria for the leptonic channel are defined to be completely orthogonal to the hadronic channel by inverting the lepton veto i.e. requiring at least one isolated lepton in the event. Finally, only 2 jets are required, satisfying the criteria discussed above.

To improve the signal-to-background ratio, two boosted decision tree (BDT) classifiers are trained independently in each channel. The classifiers aim to distinguish between signal-like and background-like events, using input variables related to the kinematics of the event con-

Table 1: Summary of the input variables for both the hadronic and leptonic BDT classifiers.

Description	Hadronic	Leptonic
Leading and sub-leading photon variables	$p_{\mathrm{T}}^{\gamma(1/2)}/m_{\gamma\gamma}$, $\eta^{\gamma(1/2)}$	$p_{\mathrm{T}}^{\gamma(1/2)}/m_{\gamma\gamma}$, $\eta^{\gamma(1/2)}$
Leading and sub-leading photon isolation variables	$\sum_{\Delta R_\gamma<0.4} p_{\mathrm{T}}^{\mathrm{charged}}/p_{\mathrm{T}}^{\gamma}$	$\sum_{\Delta R_\gamma<0.4} p_{\mathrm{T}}^{\mathrm{charged}}/p_{\mathrm{T}}^{\gamma}$
Leading jet kinematics	$p_{\mathrm{T}}^{\mathrm{j1/j2/j3/j4}}$, $\eta^{\mathrm{j1/j2/j3/j4}}$	$p_{\mathrm{T}}^{\mathrm{j1/j2/j3}}$, $\eta^{\mathrm{j1/j2/j3}}$
Leading lepton kinematics	-	p_{T}^{ℓ}, η^{ℓ}
Missing transverse momentum	$\lvert p_{\mathrm{T}}^{\mathrm{miss}}\rvert$	$\lvert p_{\mathrm{T}}^{\mathrm{miss}}\rvert$
Scalar sum of all energy, mitigating the effect of pile-up	S_T	S_T
Minimum difference in azimuthal angle between the diphoton system and object	Closest jet: $\Delta\phi_{\gamma\gamma,\mathrm{j}}$	Leading lepton: $\Delta\phi_{\gamma\gamma,\ell}$
Global variables	N_{jets}, $N_{\mathrm{b\text{-}jets}}$	N_{jets}, $N_{\mathrm{b\text{-}jets}}$, N_{leptons}

stituents. Importantly, variables directly related to the external Higgs boson kinematics, such as diphoton rapidity, are avoided to minimise distortions to the $p_{\mathrm{T}}^{\mathrm{H}}$ spectrum. Variables related to the photon quality were included in the BDT classifiers for the ttH selection in the Run II $\mathrm{H} \to \gamma\gamma$ analysis [48]. However, such variables, which are not available in DELPHES, are less effective at separating signal and background than the kinematicic ones. Therefore, the additional sensitivity gained by including photon quality variables is expected to be small. In training, ttH and tH are classified as signal, and ggH and VH events are included in the definition of background. The input variables for both the hadronic and leptonic BDTs are summarised in Table 1.

Figure 2 shows the respective BDT outputs for events in the hadronic and leptonic channels, after pre-selection. For the differential cross section measurement, it is necessary to select a relatively loose working point to maintain a high signal acceptance and thus obviate a large unfolding of the selection process. Events are required to have a BDT output value greater than 0.28 (0.13) in the hadronic (leptonic) selection. Tables 2 and 3 show the event yields at each stage of selection, for the hadronic and leptonic channels respectively. The yields are separated according to process, and all values are normalised to $3\,\mathrm{ab}^{-1}$.

5 Event categorisation and signal and background modelling

Table 4 lists the bins in $p_{\mathrm{T}}^{\mathrm{H}}$ in which the ttH + tH differential cross section is measured. This binning scenario is chosen to match the CMS + ATLAS agreed bin boundaries for inclusive p_T^H differential measurements [49]. The simulated Higgs boson signal and background events which pass the selection are divided into bins of $p_{\mathrm{T}}^{\gamma\gamma}$, whose boundaries correspond to those listed in Table 4. In the hadronic channel, all except the highest $p_{\mathrm{T}}^{\gamma\gamma}$ bin, are further split into two categories according to the hadronic BDT output. The boundary is chosen at a BDT output value of 0.61, which effectively splits each bin into a low and high ttH purity category. This is not possible in the [350,∞] GeV bin due to limited data sample size.

For each event category, the Higgs boson signal events in that category are further divided into the contributions from different $p_{\mathrm{T}}^{\mathrm{H}}$ bins and according to their production mechanism. Due to the excellent photon energy resolution, each $p_{\mathrm{T}}^{\gamma\gamma}$ category is dominated by events from the corresponding $p_{\mathrm{T}}^{\mathrm{H}}$ bin. The events are then fit using a parametric model, constructed using a

Table 2: Number of events remaining at the subsequent stages of the ttH + tH hadronic selection. Also shown are the respective efficiencies of selection at each stage. The BDT efficiency, ϵ_{BDT}, is defined as the ratio of the number of events remaining after the cut on the BDT output, to the number of events remaining after pre-selection. All event yields are normalised to $3\,\mathrm{ab}^{-1}$.

	Pre-selection	BDT (>0.28)	ϵ_{pre}	ϵ_{BDT}	ϵ_{tot}
ttH	820	650	20%	79%	16%
tH	140	80	19%	57%	11%
ggH	860	220	0.23%	25%	0.06%
VH	170	43	1.1%	25%	0.27%
$\gamma-\gamma$	2.1×10^{5}	2.1×10^{4}	0.07%	10%	7.1×10^{-5}
$\gamma-\mathrm{j}$	8.8×10^{4}	4100	2.8×10^{-5}	4.7%	1.3×10^{-6}
$\mathrm{tt}+\gamma\gamma$	340	244	0.56%	71%	0.40%
$\mathrm{tt}+\gamma$	5100	2700	0.08%	54%	0.04%
$\mathrm{t\bar{t}}$	3.1×10^{4}	1.3×10^{4}	1.2×10^{-5}	43%	5.2×10^{-6}
$\mathrm{t}+\gamma+\mathrm{j}$	3800	780	0.11%	21%	0.02%
Total Bkgd	3.4×10^{5}	4.3×10^{4}	1.0×10^{-4}	13%	1.3×10^{-5}

Table 3: Number of events remaining at the subsequent stages of the ttH + tH leptonic selection. Also shown are the respective efficiencies of selection at each stage. The BDT efficiency, ϵ_{BDT}, is defined as the ratio of the number of events remaining after the cut on the BDT output, to the number of events remaining after pre-selection. All event yields are normalised to $3\,\mathrm{ab}^{-1}$.

	Pre-selection	BDT (>0.13)	ϵ_{pre}	ϵ_{BDT}	ϵ_{tot}
ttH	380	290	9.1%	77%	7.0%
tH	45	32	6.1%	72%	4.4%
ggH	18	2.0	4.7×10^{-5}	11%	5.2×10^{-6}
VH	23	11	0.15%	46%	0.07%
$\gamma-\gamma$	6500	1400	2.3×10^{-5}	22%	5.0×10^{-6}
$\gamma-\mathrm{j}$	1100	157	3.5×10^{-7}	14%	5.0×10^{-8}
$\mathrm{tt}+\gamma\gamma$	630	390	1.0%	62%	0.63%
$\mathrm{tt}+\gamma$	2900	1100	0.08%	40%	0.03%
$\mathrm{t\bar{t}}$	8400	2500	9.0×10^{-5}	30%	2.7×10^{-5}
$\mathrm{t}+\gamma+\mathrm{j}$	780	100	0.02%	13%	2.6×10^{-5}
Total Bkgd	2.0×10^{4}	5700	6.2×10^{-6}	28%	1.7×10^{-6}

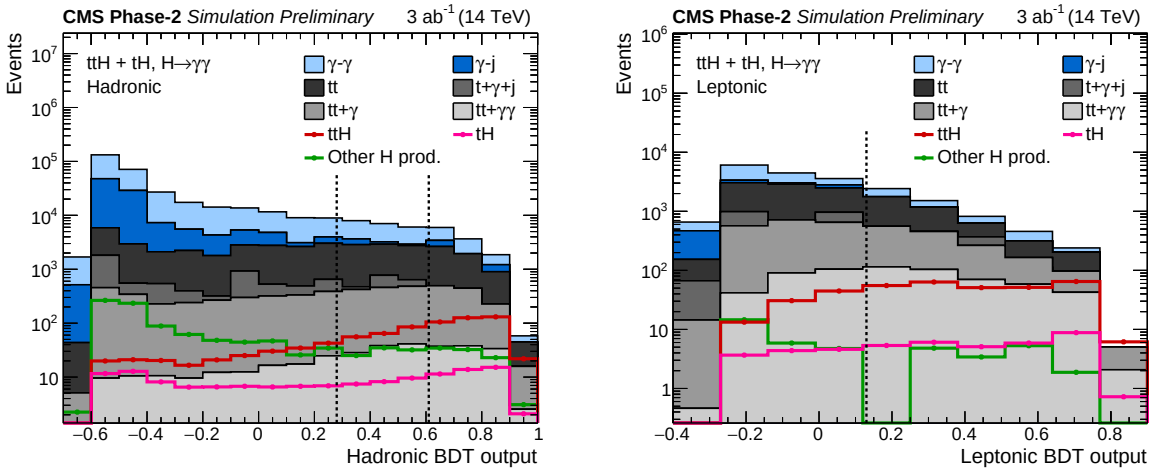

Figure 2: The BDT output distributions for the hadronic (left) and leptonic (right) channels, after pre-selection has been applied. Events with a BDT output value greater than 0.28 (0.13) are selected for the hadronic (leptonic) categories. This selection boundary is indicated by the leftmost (single) dashed line in the hadronic (leptonic) BDT output distribution. The second dashed line in the hadronic BDT output distribution shows the additional boundary at 0.61, which is used to further split the hadronic categories according to high and low ttH purity.

Table 4: The kinematic bins in which the differential cross sections are measured.

Variable	bins [GeV]						
$p_{\mathrm{T}}^{\mathrm{H}}$	0	45	80	120	200	350	∞

sum of Gaussian probability density functions of the invariant diphoton mass $m_{\gamma\gamma}$. This model is sufficient to describe the mass resolution and peak position in each of the event categories while providing a smooth functional form. The simulated background events in each category are fit using a set of smoothly falling functions in $m_{\gamma\gamma}$. The normalisations for the signal and background models are defined as the sum of weights of the simulated signal (separated into $p_{\mathrm{T}}^{\mathrm{H}}$ bins and production processes) or background events which contribute.

The sum of the fitted signal and background functions are shown for each category in Figs. 3, 4 and 5. The signal component due to ttH and tH only is also shown. A pseudo-data set is generated from the fitted distributions, and overlaid to illustrate a representative data sample which can be expected with 3 ab^{-1} at the HL-LHC assuming SM Higgs boson production.

- *Integrated luminosity*: amounts to a flat 1% uncertainty in the yield in each (i,j,k) combination.
- *Photon identification efficiency*: this uncertainty is expected to improve with respect to the LHC Run II value. To accommodate this, a flat 0.5% uncertainty is used for all photons, irrespective of pseudorapidity. Assuming a uniform photon identification efficiency across all regions of the detector of 80%, and accounting for the fact that two photons are required in the selection, amounts to a 1.3% yield uncertainty for each (i,j,k) combination.
- *Jet energy scale*: the uncertainty in the jet energy scale depends on the measured transverse momentum of the jet and varies between 0.5-3%. The p_T of all jets, in all signal samples, are scaled both up and down according to the uncertainty for the respective jet p_T. The scaled samples are subsequently propagated through the

selection process, and the yield uncertainty is realised by comparing the scaled yield to the nominal yield in each (i,j,k) combination. This corresponds to an average yield uncertainty, across all combinations, between 2-3%.

- *b tagging efficiency*: a weight is applied to each event, according to the number of true b-jets at generator-level. The weight parametrises the increase/decrease in the signal yield realised at the $\pm 1\sigma$ bounds of the uncertainty in the b tagging efficiency, at the medium (with MTD) working point. The reweighted samples are propagated through the selection process, and the (i,j,k) yield uncertainty is determined by comparing the reweighted yields to the nominal yield. This provides an average yield uncertainty between 0-1%.
- *Theoretical uncertainties in the ggH yield*: a number of uncertainties are incorporated to account for the overall normalisation of the ggH production mode, as well as the migration of ggH events between (i,ggH,k) combinations. The yield variations are calculated according to the 2017 recommendations of the LHC Higgs Cross Section Working Group [37]. Events are reweighted, both up and down, according to uncertainties related to the QCD scale, the number of jets, the transverse momentum of the Higgs boson, and top mass effects. The reweighted events are propagated through selection, and the yield uncertainties are calculated as the ratio of the reweighted yields to the nominal yields in each (i,ggH,k) combination. The uncertainties, at most, provide a 15% variation in the yield for a given (i,ggH,k) combination.
- *Theoretical uncertainties in the inclusive ttH, tH and VH cross sections*: these uncertainties are implemented as yield uncertainties in all (i,j,k) combinations, for the ttH, tH and VH production modes. The values are taken directly from the LHC Higgs Cross Section Working Group, and are separated into the effects from the uncertainties in the factorisation and renormalisation scales, the parton distribution function (PDF), and the strong coupling constant, α_s. The uncertainties in the QCD scales dominate, and after scaling down by 50%, yield variations are found to be less than 2.5% for VH, 5% for ttH and 7.5% for tH.
- *Theoretical uncertainties related to the shape of the p_T^H spectrum*: the shape effects, originating from the uncertainty in the factorisation and renormalisation scales, are included for the ttH and tH production modes. Events are reweighted, on an event-by-event basis, for the situation where the renormalisation and factorisation scales are, independently, doubled and halved. These uncertainties predominanty account for the migration between p_T^H bins and the efficiency of the cut on the BDT output values. In general, the shape uncertainties have a smaller impact than the overall normalisation uncertainties.

Systematic uncertainties in the photon scale and resolution, which modify the shape of the signal models, are expected to have a small effect on the final sensitivity, and are therefore ignored in this analysis.

Since ttH + tH differential cross section measurements are statistically limited at the HL-LHC, only the dominant systematic uncertainties in such measurements are considered. These are incorporated into the signal models as nuisance parameters, $\vec{\theta}_s$, and are treated as log-normal variations in the yield of a particular (i,j,k) signal combination, where i labels the $p_{\mathrm{T}}^{\mathrm{H}}$ bin, j labels the production mode, and k corresponds to the reconstruction-level category. The systematic uncertainties considered are in line with the recommendations for HL-LHC projections [50], and are as listed below. All theoretical uncertainties are reduced by 50%, with respect to the Run II values, to represent improvements in theoretical predictions.

6 Results

6.1 Differential cross section measurements

The differential ttH + tH production cross section of ttH + tH production is determined by defining a scaling parameter, μ_i, for each bin, i, in $p_{\mathrm{T}}^{\mathrm{H}}$ such that the signal model, S_k^{ij}, scales according to,

$$S_k^{ij}(\mu_i, \vec{\theta}_s) = \mu_i \times S_k^{ij}(\vec{\theta}_s)\Big|_{\mu_i=1} \qquad \forall \text{ categories } k \text{ and } j = (\mathrm{ttH}, \mathrm{tH}). \tag{1}$$

A likelihood function is constructed in each category, using the signal and background models and an asimov dataset assuming that all $\mu_i = 1$. The product over all of these likelihoods is used to construct a profiled likelihood ratio test-statistic, to determine the best-fit values and uncertainties for each μ_i, as described in Ref. [10]. The parameters of the background functions are profiled as nuisance parameters to model the statistical precision with $3\,\mathrm{ab}^{-1}$ of data [48]. The fitted values of μ_i and their respective uncertainties are converted to fiducial cross sections times branching ratios, $\sigma_{\mathrm{fid}}^{\mathrm{ttH+tH}} \times \mathrm{BR}(H \to \gamma\gamma)$, by correcting for the effects of the event selection. The fiducial region is defined by the following criteria:

- Higgs boson rapidity: $|Y^H| < 2.5$.
- Two photons from the Higgs boson decay: $p_{\mathrm{T}}^{\gamma} > 20\,\mathrm{GeV}$ and $|\eta^{\gamma}| < 2.5$.
- At least two jets: $p_{\mathrm{T}}^{\mathrm{j}} > 25\,\mathrm{GeV}$ and $|\eta^{\mathrm{j}}| < 4$.
- At least one of the jets, satisfying the above criteria, originates from a b quark.

Around 0.7% and 0.4% of the simulated ttH + events that pass the full event selection are not contained in the fiducial region, in the hadronic and leptonic categories, respectively. Although these events are included in the likelihood function as part of the signal component, they are subtracted when calculating the fiducial cross-section.

For each $p_{\mathrm{T}}^{\mathrm{H}}$ bin, i, we define selection efficiencies, ϵ_{sel}, for the hadronic (H) and leptonic (L) channels as:

$$\epsilon_{\mathrm{sel,H/L}}^{i} = \frac{N_{\mathrm{obs,H/L}}^{i}}{N_{\mathrm{fid}}^{i}} = \frac{\mu_i \times N_{\mathrm{exp,H/L}}^{i}}{N_{\mathrm{fid}}^{i}}, \tag{2}$$

where N_{fid}^{i} is the number of simulated ttH + tH events passing the fiducial selection, in the i^{th} $p_{\mathrm{T}}^{\mathrm{H}}$ bin. The value of $N_{\mathrm{exp,H/L}}^{i}$ is determined as the number of ttH + tH events expected in the SM after the selection. The fiducial cross section times branching ratio in bin i is given by,

$$\left[\sigma_{\mathrm{fid}}^{\mathrm{ttH+tH}} \times \mathrm{BR}(H \to \gamma\gamma)\right]_i = \frac{N_{\mathrm{fid}}^{i}}{\mathcal{L}_{\mathrm{int}}}. \tag{3}$$

Figure 6 shows the expected ttH + tH differential cross sections times branching ratio, for the fiducial phase space defined above, in bins of $p_{\mathrm{T}}^{\mathrm{H}}$. The error bars represent the combined statistical and systematics uncertainties. With $3\,\mathrm{ab}^{-1}$ of HL-LHC data, uncertainties of 20-40% in the differential cross sections are expected. To separate the contribution of the hadronic

and leptonic channels, analogous likelihood scans are performed, using only the relevant categories. The hadronic channel is observed to provide, in general, greater sensitivity in terms of the differential cross section measurements due to a larger absolute signal yield after selection, compared to the leptonic channel. Additionally, the expected differential cross sections times branching ratio for anomalous values of the Higgs self coupling, κ_λ = 10 and κ_λ = -5 are shown.

6.2 Constraints on κ_λ

In order to extract the sensitivity to the Higgs boson self-coupling, we make the substitution $\mu_i \to \mu_{ij}(\kappa_\lambda)$. The parameterisations $\mu_{ij}(\kappa_\lambda)$ are determined using the electroweak reweighting tool provided in Ref. [21], which allows one to account for kinematic variations in the modifications to Higgs boson production due to non SM values of the Higgs boson self-coupling. For the contribution of ggH and to model the effect on the $H \to \gamma\gamma$ decay rate, the scaling functions calculated for inclusive events provided in Ref. [15] are used directly.

A scan of the profiled likelihood, as a function of κ_λ, is shown in Fig. 7. In the scan, all other couplings are fixed to the SM predictions. The scan is performed in the region $\kappa_\lambda \in [-10, 20]$, beyond which, the physics model used here is no longer valid as next-to-next-to-leading order effects become important. Also shown are the results when only including the hadronic or leptonic categories in the scan, to demonstrate the relative contributions from each channel. It is observed that both channels contribute significantly towards the final sensitivity. For negative values of κ_λ, larger deviations in the ttH + tH differential cross section are expected compared to positive values. The feature in the region around $5 < \kappa_\lambda < 15$ is a result of the degeneracy in the physics model. For the ttH production mode there exists a turning point in $\mu_{ij}(\kappa_\lambda)$, in this region, such that $\mu_{ij}(\kappa_\lambda)$ can take the same value for different κ_λ. This degeneracy is somewhat alleviated by the contamination of ggH in the signal model, which has a different scaling behaviour.

The individual contributions of the statistical and systematic uncertainties are determined by performing a likelihood scan with all systematic uncertainties removed. The only considerable deviation from the statistical-uncertainty-only curve, occurs in the $\kappa_\lambda \gtrsim 5$ region. This is a result of the theoretical uncertainties in the Higgs boson production yields, which have a larger effect in this region due to the degeneracy in the physics model. Using the profiled likelihood scan, values of κ_λ outside of the range $-4.1 < \kappa_\lambda < 14.1$ can be expected to be excluded at the 95% confidence level with $3\,\text{ab}^{-1}$ of data at the HL-LHC. The effect of additional fake photons, which may not be well modelled in DELPHES, is found to weaken the constraint at the 95% confidence level by around 10%.

Table 5 shows the 68% and 95% confidence level intervals for κ_λ, for different integrated luminosities recorded by the CMS Phase-2 detector at the HL-LHC, assuming constant detector performance. The intervals are extracted using the procedure described above, where the signal and background models are scaled, in each reconstruction level category, to different integrated luminosities. As the integrated luminosity increases, the constraint for positive values of κ_λ improves more dramatically than for negative values.

Additionally, a two-dimensional likelihood scan is performed, in which an overall normalisation parameter for the Higgs boson signal processes, μ_H, is profiled. This incorporates other beyond-the-standard model effects, such as an anomalous top-Higgs coupling, which in general cause an inclusive shift across the whole p_T^H spectrum. Figure 8 shows the results of the two-dimensional scan, in terms of the 68% and 95% confidence level contours. It can be seen that differential cross section measurements still provide sensitivity to κ_λ, without exploiting the overall normalisation of the p_T^H spectrum. Table 6 shows the 1σ uncertainties in μ_H and the

Table 5: The 68% and 95% confidence level intervals for κ_λ for different integrated luminosities recorded by the CMS Phase-2 detector at the HL-LHC, assuming constant detector performance. The 95% upper limit for $\mathcal{L}_{\text{int}} = 1\,\text{ab}^{-1}$ goes outside of the valid region, and is specified as 20+ in the table.

$\mathcal{L}_{\text{int}}$ (ab^{-1})	68% interval	95% interval
1	[-3.1,10.9]	[-6.2,20+]
2	[-2.2,6.5]	[-4.6,17.0]
3	[-1.9,5.3]	[-4.1,14.1]

95% confidence level intervals for κ_λ, when both profiling the other parameter and fixing the other parameter to the SM prediction.

Table 6: The 1σ uncertainties in μ_H and the 95% confidence level intervals for κ_λ, when the other parameter is profiled or fixed to the SM prediction.

Other parameter	$\mu_H \pm \sigma_{\mu_H}$	95% interval on κ_λ
Profile (κ_λ or μ_H)	$1.00^{+0.16}_{-0.11}$	[-7.7,14.1]
Fix to SM (κ_λ or μ_H)	$1.00^{+0.08}_{-0.08}$	[-4.1,14.1]

As has been detailed in other studies, the combination of multiple production and decay channels will significantly improve the overall sensitivity to the Higgs boson self-coupling via single Higgs boson production measurements [15, 16, 19].

7 Conclusions

The precision of ttH + tH, H $\to \gamma\gamma$ differential cross section measurements, at the HL-LHC with the CMS Phase-2 detector, have been determined as a function of p_T^H. The analysis has been conducted using a simulated event sample corresponding to $3\,\text{ab}^{-1}$ of pp collision data under HL-LHC conditions. A combination of the hadronic and leptonic top decay channels is performed to maximise the sensitivity of the cross section measurements to the Higgs boson self-coupling. With the data expected by the end of the HL-LHC, the cross section in bins of p_{T}^{H} can be measured within uncertainties of 20–40%, depending on the p_{T} range. When deviations from the standard model prediction for the ttH + tH p_{T}^{H} differential cross section are interpreted as modifications of the Higgs boson self-coupling, κ_λ, these measurements exclude values outside of the range -4.1 $< \kappa_\lambda <$ 14.1, at the 95% confidence level. Furthermore, it has been shown such measurements still provide sensitivity to κ_λ, without exploiting the overall normalisation of the p_{T}^{H} spectrum, thus allowing for other effects, such as the presence of anomalous top-Higgs couplings. This property is unique to differential cross section measurements.

This analysis indicates that additional sensitivity to the Higgs boson self-coupling is available through studies of the differential cross section of single Higgs boson production in association with top quarks. It should be noted that the ultimate sensitivity to the Higgs boson self-coupling, achievable at the HL-LHC, will result from a combination of analyses such as that described in this note with other Higgs decay channels and production modes, and with direct searches for double Higgs boson production.

References

[1] F. Englert and R. Brout, "Broken symmetry and the mass of gauge vector mesons", *Phys. Rev. Lett.* **13** (1964) 321, doi:10.1103/PhysRevLett.13.321.

[2] P. W. Higgs, "Broken symmetries, massless particles and gauge fields", *Phys. Lett.* **12** (1964) 132, doi:10.1016/0031-9163(64)91136-9.

[3] P. W. Higgs, "Broken symmetries and the masses of gauge bosons", *Phys. Rev. Lett.* **13** (1964) 508, doi:10.1103/PhysRevLett.13.508.

[4] G. S. Guralnik, C. R. Hagen, and T. W. B. Kibble, "Global conservation laws and massless particles", *Phys. Rev. Lett.* **13** (1964) 585, doi:10.1103/PhysRevLett.13.585.

[5] P. W. Higgs, "Spontaneous symmetry breakdown without massless bosons", *Phys. Rev.* **145** (1966) 1156, doi:10.1103/PhysRev.145.1156.

[6] T. W. B. Kibble, "Symmetry breaking in non-Abelian gauge theories", *Phys. Rev.* **155** (1967) 1554, doi:10.1103/PhysRev.155.1554.

[7] ATLAS Collaboration, "Observation of a new particle in the search for the standard model Higgs boson with the ATLAS detector at the LHC", *Phys. Lett. B* **716** (2012) 1, doi:10.1016/j.physletb.2012.08.020, arXiv:1207.7214.

[8] CMS Collaboration, "Observation of a new boson at a mass of 125 GeV with the CMS experiment at the LHC", *Phys. Lett. B* **716** (2012) 30, doi:10.1016/j.physletb.2012.08.021, arXiv:1207.7235.

[9] CMS Collaboration, "Observation of a new boson with mass near 125 GeV in pp collisions at $\sqrt{s}$ = 7 and 8 TeV", *JHEP* **06** (2013) 81, doi:10.1007/JHEP06(2013)081, arXiv:1303.4571.

[10] ATLAS and CMS Collaborations, "Measurements of the Higgs boson production and decay rates and constraints on its couplings from a combined ATLAS and CMS analysis of the LHC pp collision data at $\sqrt{s}$ = 7 and 8 TeV", *JHEP* **08** (2016) 45, doi:10.1007/JHEP08(2016)045, arXiv:1606.02266.

[11] ATLAS Collaboration, "Combined measurements of Higgs boson production and decay using up to 80 fb^{-1} of proton–proton collision data at $\sqrt{s} = 13$ TeV collected with the ATLAS experiment", Technical Report ATLAS-CONF-2018-031, CERN, Geneva, Jul, 2018.

[12] CMS Collaboration, "Combined measurements of the Higgs boson's couplings at $\sqrt{s} = 13$ TeV", Technical Report CMS-PAS-HIG-17-031, CERN, Geneva, 2018.

[13] ATLAS Collaboration, "Combination of searches for Higgs boson pairs in pp collisions at 13 TeV with the ATLAS experiment.", Technical Report ATLAS-CONF-2018-043, CERN, Geneva, Sep, 2018.

[14] CMS Collaboration, "Combination of searches for Higgs boson pair production in proton-proton collisions at $\sqrt{s} = 13$ TeV", Technical Report CMS-PAS-HIG-17-030, CERN, Geneva, 2018.

[15] G. Degrassi, P. P. Giardino, F. Maltoni, and D. Pagani, "Probing the Higgs self coupling via single Higgs production at the LHC", *JHEP* **12** (2016) 080, doi:10.1007/JHEP12(2016)080, arXiv:1607.04251.

[16] F. Maltoni, D. Pagani, A. Shivaji, and X. Zhao, "Trilinear Higgs coupling determination via single-Higgs differential measurements at the LHC", *Eur. Phys. J.* **C77** (2017), no. 12, 887, doi:10.1140/epjc/s10052-017-5410-8, arXiv:1709.08649.

[17] W. Bizon, M. Gorbahn, U. Haisch, and G. Zanderighi, "Constraints on the trilinear Higgs coupling from vector boson fusion and associated Higgs production at the LHC", *JHEP* **07** (2017) 083, doi:10.1007/JHEP07(2017)083, arXiv:1610.05771.

[18] M. Gorbahn and U. Haisch, "Indirect probes of the trilinear Higgs coupling: $gg \to h$ and $h \to \gamma\gamma$", *JHEP* **10** (2016) 094, doi:10.1007/JHEP10(2016)094, arXiv:1607.03773.

[19] S. Di Vita et al., "A global view on the Higgs self-coupling", *JHEP* **09** (2017) 069, doi:10.1007/JHEP09(2017)069, arXiv:1704.01953.

[20] M. McCullough, "An Indirect Model-Dependent Probe of the Higgs Self-Coupling", *Phys. Rev.* **D90** (2014), no. 1, 015001, doi:10.1103/PhysRevD.90.015001,10.1103/PhysRevD.92.039903, arXiv:1312.3322.

[21] A. Shivaji and X. Zhao, "Higgs Trilinear self-coupling determination through one-loop effects". https://cp3.irmp.ucl.ac.be/projects/madgraph/wiki/HiggsSelfCoupling, 2018. [Online; accessed 12-Sep-2018].

[22] CMS Collaboration, "Observation of $t\bar{t}H$ production", *Phys. Rev. Lett.* **120** (2018) 231801, doi:10.1103/PhysRevLett.120.231801, arXiv:1804.02610.

[23] ATLAS Collaboration, "Observation of Higgs boson production in association with a top quark pair at the LHC with the ATLAS detector", *Phys. Lett.* **B784** (2018) 173–191, doi:10.1016/j.physletb.2018.07.035, arXiv:1806.00425.

[24] CMS Collaboration, "The CMS experiment at the CERN LHC", *JINST* **3** (2008) S08004, doi:10.1088/1748-0221/3/08/S08004.

[25] G. Apollinari et al., "High-Luminosity Large Hadron Collider (HL-LHC) : Preliminary Design Report", doi:10.5170/CERN-2015-005.

[26] D. Contardo et al., "Technical Proposal for the Phase-II Upgrade of the CMS Detector",.

[27] CMS Collaboration, "The Phase-2 Upgrade of the CMS Tracker", Technical Report CERN-LHCC-2017-009. CMS-TDR-014, CERN, Geneva, June, 2017.

[28] CMS Collaboration, "The Phase-2 Upgrade of the CMS Barrel Calorimeter", Technical Report CERN-LHCC-2017-011. CMS-TDR-015, CERN, Geneva, Sep, 2017.

[29] CMS Collaboration, "The Phase-2 Upgrade of the CMS Endcap Calorimeter", Technical Report CERN-LHCC-2017-023. CMS-TDR-019, CERN, Geneva, Nov, 2017.

[30] CMS Collaboration, "The Phase-2 Upgrade of the CMS Muon Detectors", Technical Report CERN-LHCC-2017-012. CMS-TDR-016, CERN, Geneva, Sep, 2017.

[31] CMS Collaboration, "Technical proposal for a MIP timing detector in the CMS experiment phase 2 upgrade", Technical Report CERN-LHCC-2017-027. LHCC-P-009, CERN, Geneva, Dec, 2017.

[32] CMS Collaboration, "CMS Phase-2 Object Performance", (2018). CMS Physics Analysis Summary, in preparation.

[33] S. Alioli, P. Nason, C. Oleari, and E. Re, "A general framework for implementing NLO calculations in shower monte carlo programs: the POWHEG BOX", *JHEP* **06** (2010) 043, doi:10.1007/JHEP06(2010)043, arXiv:1002.2581.

[34] P. Nason and C. Oleari, "NLO higgs boson production via vector-boson fusion matched with shower in POWHEG", *JHEP* **02** (2010) 037, doi:10.1007/JHEP02(2010)037, arXiv:0911.5299.

[35] J. Alwall et al., "The automated computation of tree-level and next-to-leading order differential cross sections, and their matching to parton shower simulations", *JHEP* **07** (2014) 079, doi:10.1007/JHEP07(2014)079, arXiv:1405.0301.

[36] T. Sjostrand, S. Mrenna, and P. Z. Skands, "A Brief Introduction to PYTHIA 8.1", *Comput. Phys. Commun.* **178** (2008) 852–867, doi:10.1016/j.cpc.2008.01.036, arXiv:0710.3820.

[37] LHC Higgs Cross Section Working Group Collaboration, "Handbook of LHC Higgs Cross Sections: 4. Deciphering the Nature of the Higgs Sector", doi:10.23731/CYRM-2017-002, arXiv:1610.07922.

[38] C. Anastasiou et al., "Higgs boson gluon–fusion production at threshold in N^3LO QCD", *Phys. Lett. B* **737** (2014) 325, doi:10.1016/j.physletb.2014.08.067, arXiv:1403.4616.

[39] T. Gleisberg et al., "Event generation with SHERPA 1.1", *JHEP* **02** (2009) 007, doi:10.1088/1126-6708/2009/02/007, arXiv:0811.4622.

[40] DELPHES 3 Collaboration, "DELPHES 3, A modular framework for fast simulation of a generic collider experiment", *JHEP* **02** (2014) 057, doi:10.1007/JHEP02(2014)057, arXiv:1307.6346.

[41] GEANT4 Collaboration, "GEANT4 – a simulation toolkit", *Nucl. Instrum. Meth. A* **506** (2003) 250, doi:10.1016/S0168-9002(03)01368-8.

[42] CMS Collaboration, "Performance of Photon Reconstruction and Identification with the CMS Detector in Proton-Proton Collisions at sqrt(s) = 8 TeV", *JINST* **10** (2015), no. 08, P08010, doi:10.1088/1748-0221/10/08/P08010, arXiv:1502.02702.

[43] CMS Collaboration, "Particle-flow reconstruction and global event description with the CMS detector", *JINST* **12** (2017), no. 10, P10003, doi:10.1088/1748-0221/12/10/P10003, arXiv:1706.04965.

[44] M. Cacciari, G. P. Salam, and G. Soyez, "The anti-k_T jet clustering algorithm", *JHEP* **04** (2008) 063, doi:10.1088/1126-6708/2008/04/063, arXiv:0802.1189.

[45] M. Cacciari, G. P. Salam, and G. Soyez, "FastJet user manual", *Eur. Phys. J. C* **72** (2012) 1896, doi:10.1140/epjc/s10052-012-1896-2, arXiv:1111.6097.

[46] D. Bertolini, P. Harris, M. Low, and N. Tran, "Pileup Per Particle Identification", *JHEP* **10** (2014) 059, doi:10.1007/JHEP10(2014)059, arXiv:1407.6013.

[47] CMS Collaboration, "Identification of heavy-flavour jets with the CMS detector in pp collisions at 13 TeV", *JINST* **13** (2018), no. 05, P05011, doi:10.1088/1748-0221/13/05/P05011, arXiv:1712.07158.

[48] CMS Collaboration, "Measurements of Higgs boson properties in the diphoton decay channel in proton-proton collisions at $\sqrt{s} = 13$ TeV", arXiv:1804.02716.

[49] CMS Collaboration, "Combined measurement and interpretation of differential Higgs boson production cross sections at $\sqrt{s}$=13 TeV", Technical Report CMS-PAS-HIG-17-028, CERN, Geneva, 2018.

[50] CMS UPSG group, "Recommendations for Systematic Uncertainties HL-LHC, 3000 fb^{-1}". https://twiki.cern.ch/twiki/bin/view/LHCPhysics/HLHELHCCommonSystematics, 2018. [Online; accessed 31 Oct. 2018].

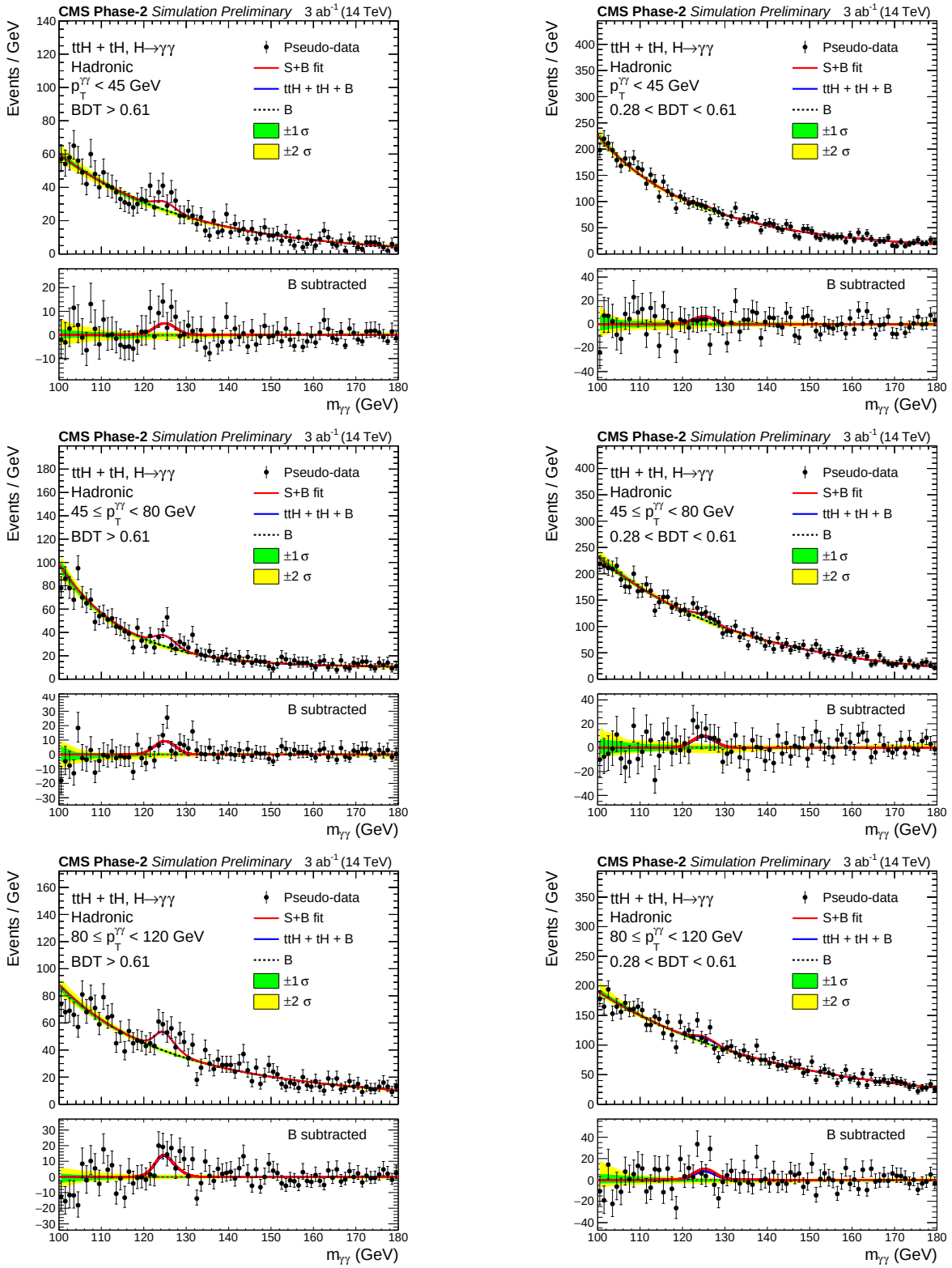

Figure 3: Best-fit signal (S) + background (B) models for the reconstruction-level categories in the ttH + tH hadronic channel, in the three lowest $p_T^{\gamma\gamma}$ bins: [0,45] GeV, [45,80] GeV and [80,120] GeV. A pseudo-data set is thrown from the best-fit functions, represented by the black points. The one (green) and two (yellow) standard deviation bands show the uncertainties in the background component of the fit. The residual plots, pseudo-data minus the background component, are shown in the lower panels.

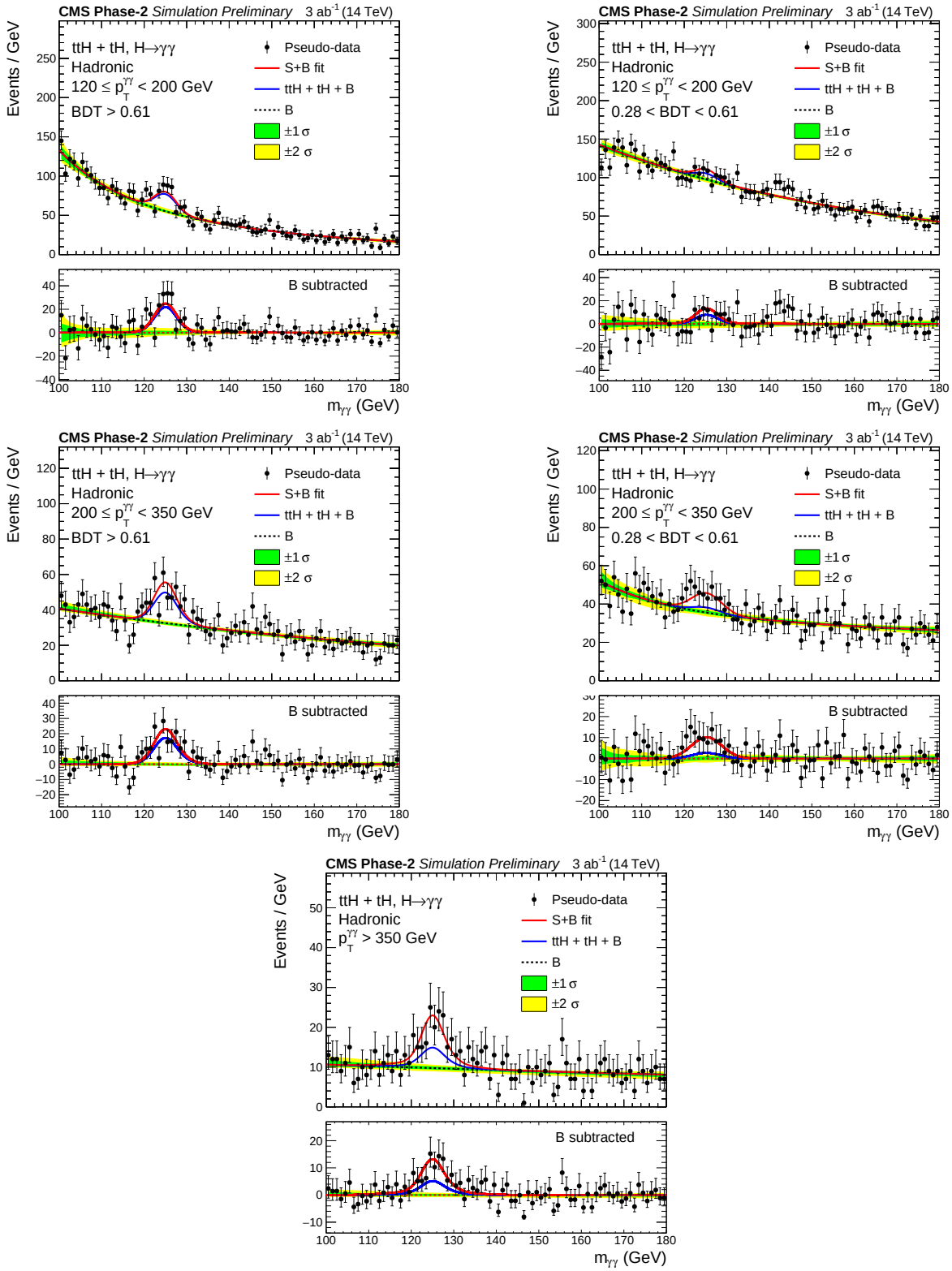

Figure 4: Best-fit signal (S) + background (B) models for the reconstruction-level categories in the ttH + tH hadronic channel, in the three highest $p_{\mathrm{T}}^{\gamma\gamma}$ bins: [120,200] GeV, [200,350] GeV and [350,∞] GeV. A pseudo-data set is thrown from the best-fit functions, represented by the black points. The one (green) and two (yellow) standard deviation bands show the uncertainties in the background component of the fit. The residual plots, pseudo-data minus the background component, are shown in the lower panels.

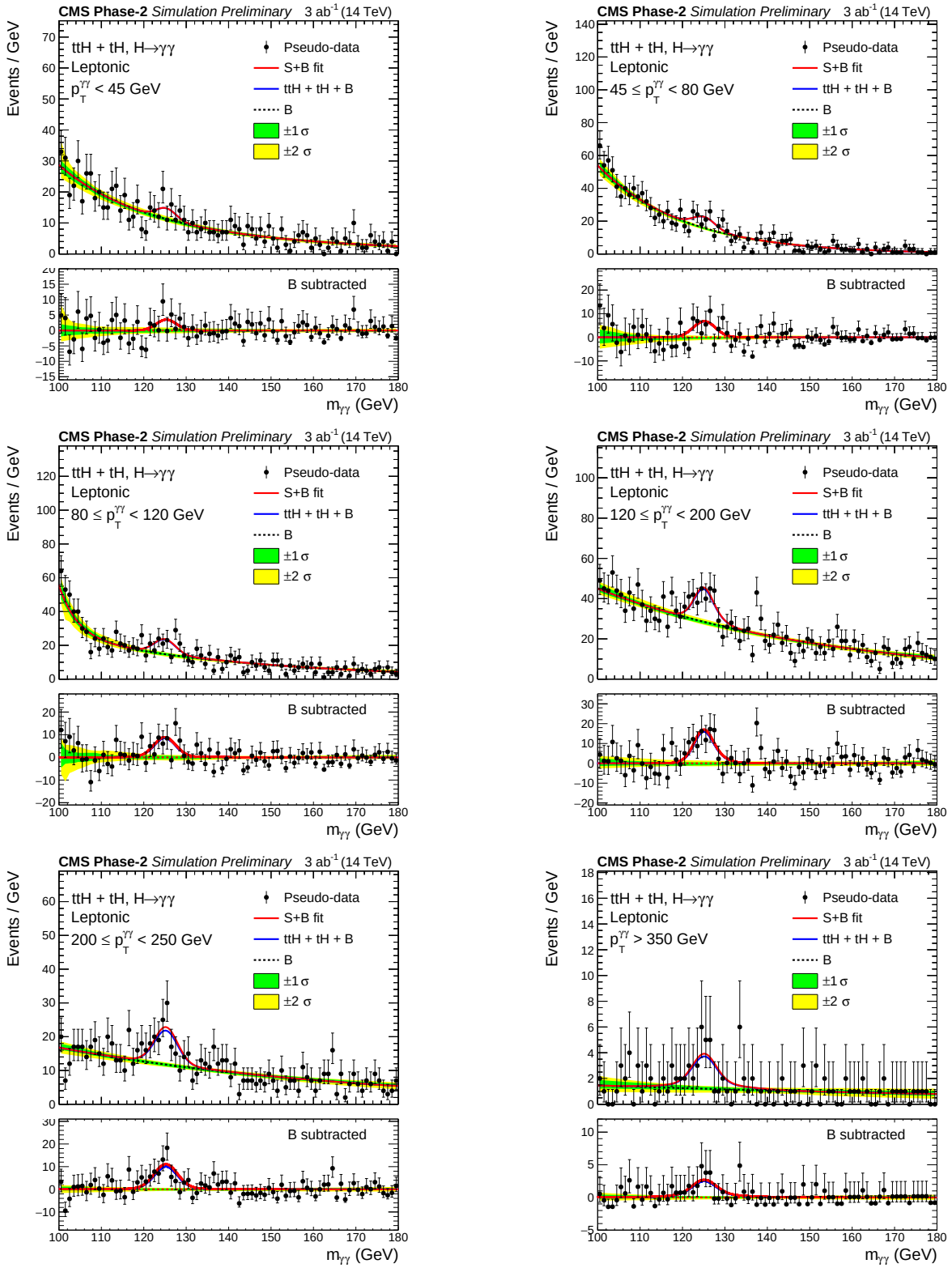

Figure 5: Best-fit signal (S) + background (B) models for each reconstruction-level category in the ttH + tH leptonic channel. A pseudo-data set is thrown from the best-fit functions, represented by the black points. The one (green) and two (yellow) standard deviation bands show the uncertainties in the background component of the fit. The residual plots, pseudo-data minus the background component, are shown in the lower panels.

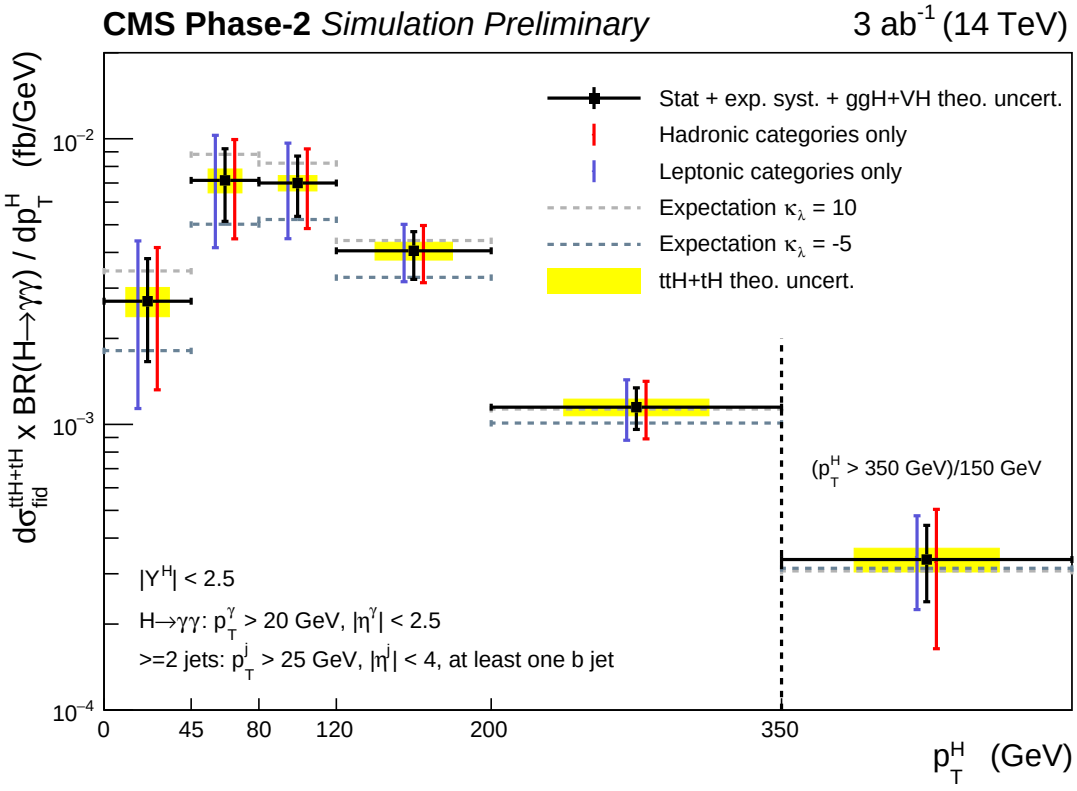

Figure 6: The expected differential ttH + tH cross sections times branching ratio, along with their respective uncertainties, in bins of $p_{\mathrm{T}}^{\mathrm{H}}$. These are for the fiducial region of phase space defined in the bottom left of the plot. The error bars on the black points include the statistical uncertainty, the experimental systematic uncertainties and the theoretical uncertainties related to the ggH and VH yields. The theoretical uncertainties in the inclusive ttH + tH cross section and those effecting the shape of the ttH + tH p_T^H spectrum, originating from the uncertainty in the QCD scales, are shown by the shaded yellow regions. Contributions from the individual hadronic and leptonic channels are shown in red and purple respectively. The cross section for the $p_{\mathrm{T}}^{\mathrm{H}}$ = [350,∞] GeV bin is scaled by the width of the previous bin. Additionally, the expected differential ttH + tH cross sections for anomalous values of the Higgs boson self-coupling (κ_λ = 10 and κ_λ = -5) are shown by the horizontal dashed lines.

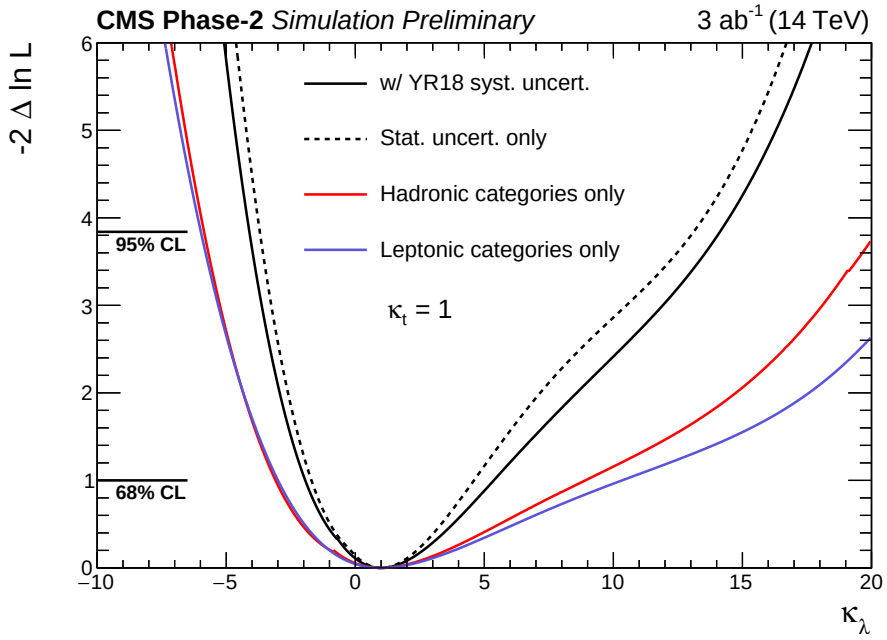

Figure 7: Results of the likelihood scan in κ_λ. The individual contributions of the statistical and systematic uncertainties are separated by performing a likelihood scan with all systematics removed. The observed deviation from the statistical uncertainty only curve is driven by the theoretical systematic uncertainties in the Higgs boson production yields. Additionally, the contributions from the hadronic and leptonic channels have been separated, shown in red and purple, respectively.

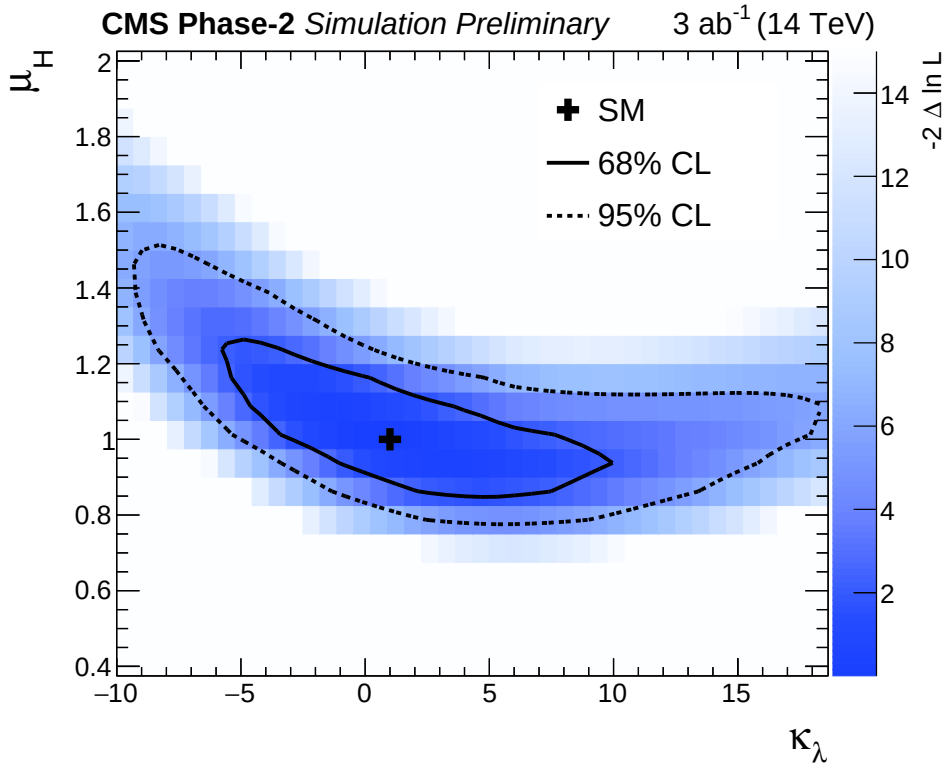

Figure 8: Results of the two-dimensional likelihood scan in κ_λ-vs-μ_{H}, where μ_{H} allows all Higgs boson production modes to scale relative to the SM prediction. The 68% and 95% confidence level contours are shown by the solid and dashed lines respectively. The SM expectation is shown by the black cross.